Acta Cryst. (1964). **17**, 973

X-ray Analysis of Ferroelectric Domains in the Paraelectric Phase of $NaNO_2$

By Marisa Canut*

Section of Crystal Thermodynamics,† Department of Crystal Physics, C.S.I.C., Madrid, Spain

and Rolf Hosemann

Fritz-Haber-Institut der Max-Planck-Gesellschaft, Berlin-Dahlem, Germany

(*Received* 8 *July* 1963)

It is well known that a paraelectric phase of $NaNO_2$ crystals exists above 160 °C. Laue patterns with filtered Cu radiation obtained at 185 °C show, besides thermodiffuse spots, diffuse but relatively sharp layer lines orthogonal to the polar axis along $l=2, 3, 4$. It is shown that they can be explained by *ca.* 30 Å long small domains with ferroelectric structure (so called "cigarrillos") statistically orientated parallel or antiparallel to the polar axis. This positional disorder with correlations can never explain the observed continuous intensity of the first layer line near 002, even if correlated librations are introduced. Calculations and Fraunhofer patterns of two-dimensional models with statistical point structures prove that the domains oscillate parallel to the polar axis as rigid entities. The diffuse spots 030, 040 can furthermore be explained by cross-vibrating linear segments of the ferroelectric domains. Much of the analysis is carried out with the help of the Q-function calculated and experimentally produced from the models with a two-dimensional folding machine.

1. Introduction

Ferroelectricity in $NaNO_2$ was revealed by the measurements of dielectric properties carried out by Sawada, Nomura, Fujii & Yoshida (1958), and since also the ferroelectric phase is stable at room temperature, interest in a closer knowledge of the mechanism of the ferroelectric–paraelectric transition has grown rapidly. Many papers have been published in connection with $NaNO_2$ and a number of characteristics have been determined.

The crystal symmetry of $NaNO_2$ at room temperature is orthorhombic, space group $Imm2$; its structure was determined by Ziegler (1931) and subsequently refined by Carpenter (1952, 1955), Truter (1954) and Kay & Frazer (1961). The unit cell contains two $NaNO_2$ molecules and has a polar axis along the [001] direction (Carpenter's unit-cell choice) which is also the direction of spontaneous polarization. The atomic arrangement in the unit cell at room temperature is shown schematically in Fig. 1(*a*). The lattice constants are $a_0=3{\cdot}56$, $b_0=5{\cdot}56$ and $c_0=5{\cdot}38$ Å. The crystal is composed, presumably not in the most closely-packed state, of Na^+ ions and NO_2^- ions alternately disposed

Table 1. $NaNO_2$, *ferroelectric phase. Atomic parameters for the* (100) *projection* (*Kay & Frazer*, 1961)

	y	z
Na	0	0·587
N	0	0·1180
O	0·1941	0

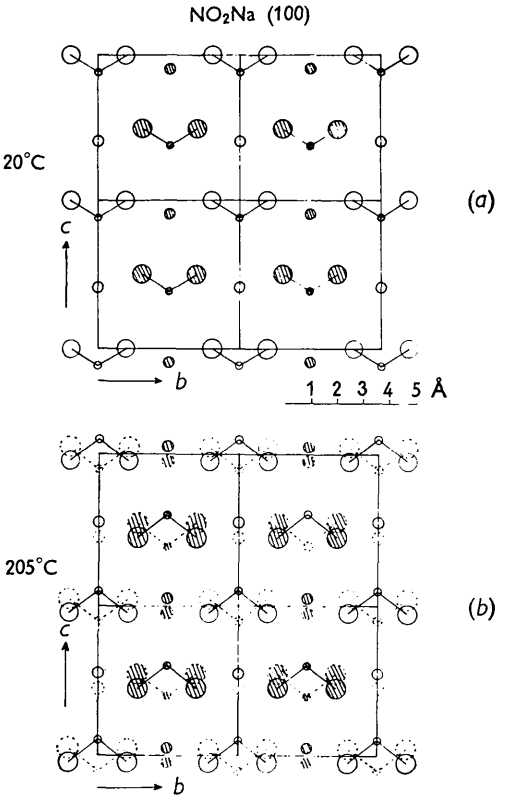

Fig. 1. $NaNO_2$. Projection of the structure on (100). (*a*) Ferroelectric phase. (*b*) Paraelectric phase (after Strijk & MacGillavry, 1943).

* Present address: School of Technology, Southern Illinois University, Carbondale, U.S.A.

† Partially supported by the U.S. Army, Contract DA-91-591-EUC-2755, through its European Office and a grant of the Technische Universität, Berlin-Charlottenburg.

along the [001] axis. The NO_2^- ion is a symmetric non-linear group and lies parallel to the (100) plane. The bisectrix of the angle ONO is aligned to the $+c$ axis. The atomic coordinates of the refined structure at room temperature are given in Table 1.

Strijk & MacGillavry (1943) found a phase transition in $NaNO_2$ at about 158 °C by piezoelectric as well as X-ray studies. The crystal gains above the Curie point a mirror plane perpendicular to the c axis (Fig. 1*b*), centers of symmetry are therefore obtained and the space group becomes *Immm*.

The exact mechanism of the phase transition still remains uncertain, but it is generally believed that the orientation of NO_2^- ions takes the most important role in the problem.

Since the NO_2 groups are asymmetric, Strijk & MacGillavry (1943) had to conclude that the mirror plane that appears in the paraelectric phase has a statistical nature. These authors (Strijk & MacGillavry, 1946) were unable to determine whether the NO_2 groups were rotating or frozen into two symmetric positions along the polar axis of the room-temperature structure.

Recently, Kay, Frazer & Ueda (1962) have refined the (100) projection of the paraelectric structure by neutron diffraction studies, and from comparison between the calculated F_{0kl} values of the models with hindered rotation of the NO_2 groups and with positional disorder, they are in favour of the disordered model. The discrepancy index obtained by these workers is $R=0{\cdot}077$. Table 2 gives the y z atomic parameters of $NaNO_2$ at 185 °C according to Kay, Frazer & Ueda (1962).

Table 2. $NaNO_2$, *paraelectric phase at* 185 °C. *Atomic parameters for the* (100) *projection**

	y	z
Na	0	0·5401
N	0	0·0725
O	0·1920	−0·0416

* Positions in *Immm*: ½ Na in 4(*g*), ½ N in 4(*g*), and ½ O in 8(*l*).

2. X-ray experimental

Single crystals of $NaNO_2$ were obtained by slow evaporation of an aqueous solution; they were elongated along [100].

X-ray Laue and oscillation photographs were taken at room temperature and at temperatures above the transition point in a Unicam camera, with a nickel furnace attached to the camera. X-ray Cu-filtered radiation was used, at the condition 20 mA, 40 kV. The exposure time of the Laue photographs was 2h, and the thickness of the crystals used about 1 mm. The temperature was measured with a copper–constantan thermocouple.

Several Laue and oscillation photographs of the series at room temperature were repeated, and Laue and oscillation photographs of the paraelectric phase at 185 °C were obtained at identical positions.

X-ray diffuse scattering of the ferroelectric phase of $NaNO_2$

Laue photographs of the ferroelectric phase of $NaNO_2$ (Fig. 2*a* and 3*a*) show the typical thermal diffuse pattern of ionic crystals, very similar to that of $NaNO_3$ (Amorós, Canut & de Acha, 1960), NH_4NO_3 (Alonso, Canut & Amorós, 1958), *etc.* The strong spots are associated with reciprocal lattice points of $|F_o|$ strong. The diffuse domains have been plotted in the reciprocal levels $[100]_0$ and $[100]_1$.

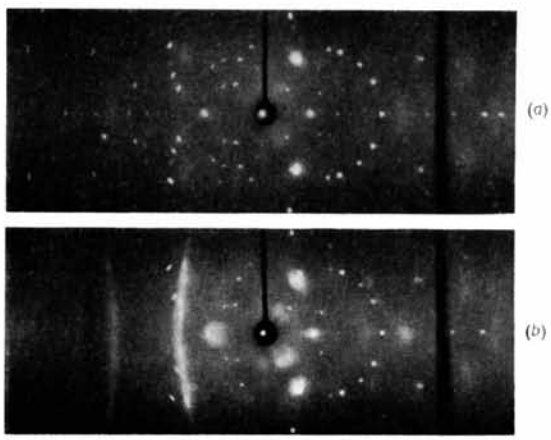

Fig. 2. $NaNO_2$. Laue photographs. [100] vertical. Cu-filtered X-radiation, X-ray beam at 20° from [001]. (*a*) Ferroelectric phase (20 °C). (*b*) Paraelectric phase (185 °C).

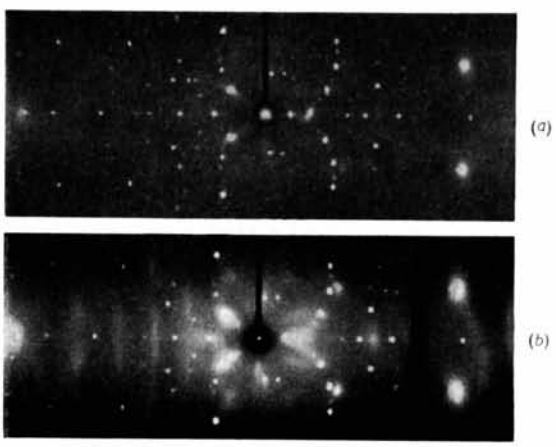

Fig. 3. $NaNO_2$. Laue photographs. [100] vertical. Cu-filtered X-radiation, X-ray beam at 30° from [001]. (*a*) Ferroelectric phase (20 °C). (*b*) Paraelectric phase (185 °C).

$[100]_0$ level: Fig. 4(*a*) shows the diffuse scattering connected with $0kl$ reciprocal lattice points. The strongest diffuse domains are associated with the reciprocal lattice points 002, 040, 022, 024 and 031 with $|F_o| > 14$. This shows the correlation between strong diffuse scattering and $|F_o|^2$. The diffuse spots are elongated in the direction of the corresponding crystallographic plane.

The extinction condition $h+k+l=2n+1$ is observed by the diffuse scattering and only some very scant

and weak diffuse streaks connecting some reciprocal lattice points appear in the Laue photographs.

It must be emphasized that the diffuse scattering of the ferroelectric phase is of thermal origin and cannot be associated with any ferroelectric effect as was suggested by Mitsui (1958). No correlation between the imaginary part B of the structure factor $F=A+iB$ and the corresponding diffuse intensity domains has been found. For instance, the Bragg intensity 004 has $B_{004}=0$ and the associated diffuse intensity is strong.

X-ray diffuse scattering of the paraelectric phase of $NaNO_2$

The diffuse scattering appearing in the Laue and oscillation photographs of the paraelectric phase clearly shows disorder diffuse scattering superimposed on the temperature diffuse scattering. Laue photographs of the ferroelectric and paraelectric phases of sodium nitrite are compared in Figs. 2 and 3. At this point it is interesting to emphasize the striking ressemblance between this disorder diffuse scattering and that of phase II of NH_4NO_3 discovered by Amorós, Alonso & Canut (1958).

The disorder scattering is distributed in sheets normal to [001], and thus combines some of the thermal diffuse domains centered at 002, 022, 004, 024, 013 or $0\bar{1}3$, 015 or $0\bar{1}5$.

In addition, two diffuse bands centered at the reciprocal lattice points 030 (forbidden) and 040 can also be seen. These bands are parallel to the polar axis. At room temperature some thermal diffuse scattering does appear, but no disorder scattering (Figs. 2*a*, 3*a*, 4*a*).

In Fig. 4(*b*) we have plotted the disordered diffuse scattering as obtained from the Laue photographs and in Fig. 4(*c*) the total diffuse scattering of the paraelectric phase.

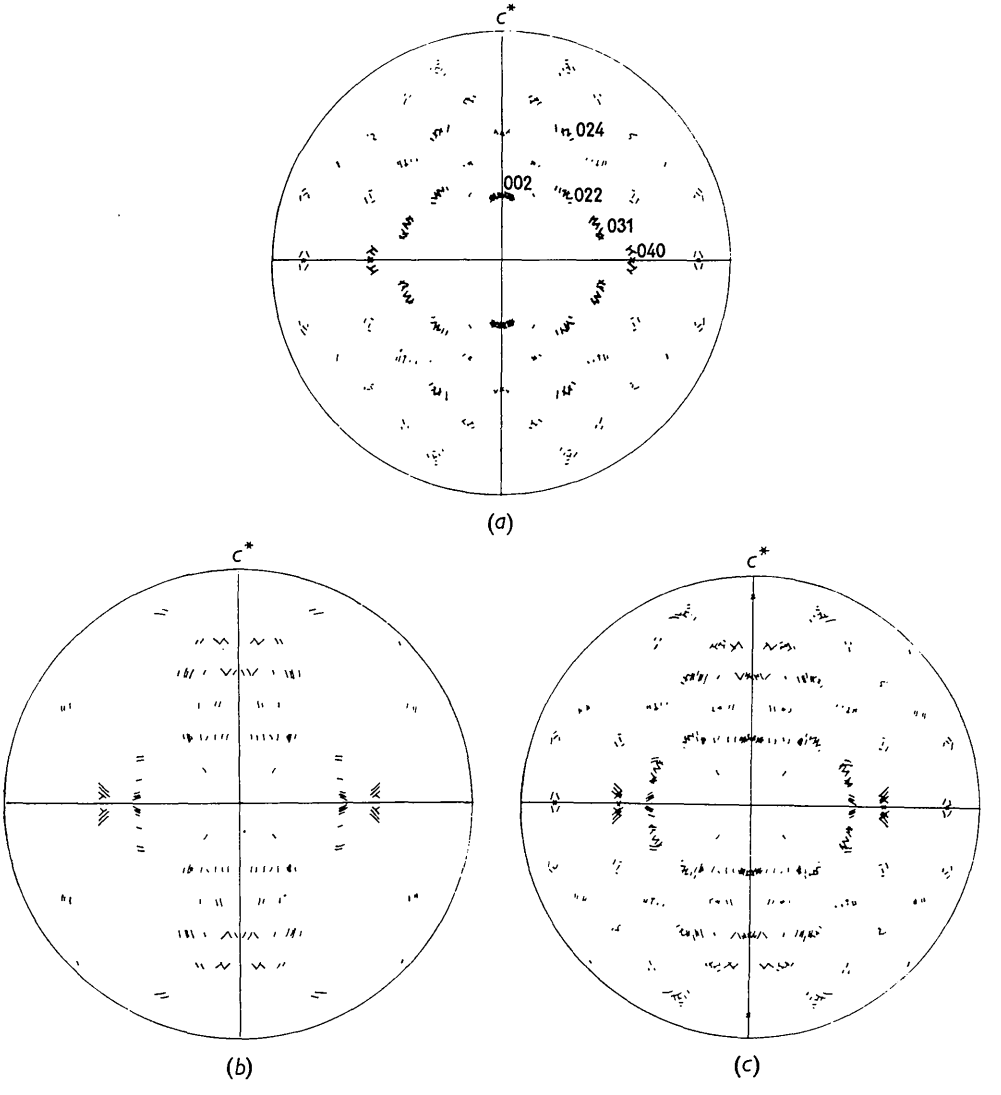

Fig. 4. $NaNO_2$. Diffuse scattering domains in $[100]_0$. (*a*) Ferroelectric phase (20 °C). (*b*) Only disorder scattering plotted (185 °C). (*c*) Disorder plus thermal scattering plotted (185 °C).

In addition to the photographic method, diffractometric measurements have been made in connection with the critical scattering studies at the transition point. The experiments given by Mendiola (1964) prove the existence of a sharp diffuse intensity sheet in the 002 plane. Along the reciprocal row $l=2$, disorder diffuse scattering above the Curie point is continuous from 002 up to at least 032 (see Fig. 10).

3. Optical

In order to understand the formation of the disorder connected with the paraelectric phase, we have decided to use an optical analogue.

An optical diffractometer and a folding apparatus described by Hosemann (1959, 1962) were used to obtain the Fraunhofer patterns and the Q functions of the different hypotheses.

The scale of the drawings of the different models was 1 Å = 4 mm and at least 20×20 unit cells were drawn, *i.e.* more than 3200 atoms. The radius R of the 'point-like' atoms was 1·2 mm, hence $\frac{1}{20}$ of a lattice cell. All atoms had the same shape, hence the same atomic scattering factor:

$$f_O^2 \sim f_N^2 \sim f_{Na}^2 = \exp(-\pi b R)^2$$

which reached half of its maximum value near the reflexions 060, 044, 006. In this way, the Fraunhofer pattern was comparable with the experimental X-ray results obtained with Cu radiation. The mask for the Fraunhofer pattern was a microfilm of the drawing at scale 1 Å = 10^{-1} mm. The two masks for the Q functions had approximately a scale of 1 Å = $4 \cdot 10^{-1}$ mm.

Firstly, a model of the ferroelectric phase was made, by using the y, z atomic coordinates and unit-cell dimensions given by Carpenter (1955). Fig. 5 shows the model of the ferroelectric phase (*a*) and the corresponding equator of the reciprocal lattice, obtained with the optical diffractometer (*b*). Four lattice cells of the Q function (in this case of the Patterson function) are shown in (*c*). The Q function is defined as the time and space average convolution square of the electron density under discussion. For ideal periodic structures it degenerates into the (unbounded) Patterson function. For point structures it has to do with the correlation functions of statistical mechanics (see for details Hosemann & Bagchi, 1962). For a structure $\varrho(x)$ not changing with time, the Q function is defined by

$$Q = \overset{2}{\sim}\varrho(x) = \int \varrho(y)\varrho(y-x)\,dy\,.$$

The optical folding machine had only a small aperture, so that a domain with a radius of about 8 Å could only be obtained in the 'vector space'. Since the model corresponds to an ideal crystal lattice, the central motif in the Q function has the same shape as the others. In (*d*) the central region of the calculated Patterson function is shown.

In the study of the paraelectric phase, two models were made, first with only NO_2 groups, *i.e.* without introducing the Na atoms into the structure. If we define the NO_2 groups as positive (NO_2^+) or negative (NO_2^-) when the vertex of the group points in the upper or lower direction, a model with statistical random distribution along the polar axis means that the same probability is given to the NO_2 groups of pointing in the positive or negative direction.

Fig. 6(*a*) (left) shows the Fraunhofer pattern of such a model. Fig. 6(*b*) (left) gives the corresponding optical Q function. The pattern at the origin of the Q function corresponds to $\overset{2}{\sim}\overline{\varrho_{NO_2}}$ and all other peaks are $\overset{2}{\sim}\overline{\varrho_{NO_2}}$. The Fourier transform of the difference between these two peaks of the Q function

$$\overset{2}{\sim}\overline{\varrho_{NO_2}} - \overset{2}{\sim}\overline{\varrho_{NO_2}} = \Delta \overset{2}{\sim}\varrho_{NO_2} \qquad (1)$$

gives rise to the continuous diffuse regions appearing in the Fraunhofer pattern of Fig. 6(*a*)

$$\mathfrak{F}(\Delta \overset{2}{\sim}\varrho_{NO_2}) = \Delta |F_{NO_2}|^2\,. \qquad (2)$$

Fig. 6(*a*) (right) shows the isodiffusion lines corresponding to $\Delta|F_{NO_2}|^2$ calculated in terms of*

$$I_{dif} = \Delta |F_{NO_2}|^2 = \overline{|F_{NO_2}|^2} - |\overline{F_{NO_2}}|^2 \qquad (3)$$

The contours correspond to values of $\Delta|F_{NO_2}|^2$ of 2·5, 5·0 and 7·5. In the figure, the reciprocal lattice points have been weighted in terms of $\overline{|F_{NO_2}|^2}$.

Fig. 6(*b*) (right) shows the central region of the calculated Q function. The central motif and the other motifs have the weights

$$\begin{array}{ccccc} & & & & \frac{1}{4} \\ & & & \frac{1}{2} & - & \frac{1}{2} \\ 1 & 1 & & \frac{1}{4} & \frac{1}{2} & \frac{1}{2} & \frac{1}{2} & \frac{1}{4} \\ 1 & 3 & 1 \quad \text{and} & \frac{1}{2} & - & \frac{3}{2} & - & \frac{1}{2} \\ 1 & 1 & & \frac{1}{4} & \frac{1}{2} & \frac{1}{2} & \frac{1}{2} & \frac{1}{4} \\ & & & & \frac{1}{2} & - & \frac{1}{2} \\ & & & & & \frac{1}{4} \end{array}$$

respectively.

A new model was drawn by introducing correlations of the NO_2 groups along the polar axis. The statistical unit of this model consists of a row of five NO_2^+ or NO_2^- groups, *i.e.* of positive or negative 'cigarrillos'. The Fraunhofer patterns and Q functions of this model are shown in Fig. 7.

The Q function of this model (Fig. 7*b*) also shows the peaks of two kinds, $\overset{2}{\sim}\overline{\varrho_{NO_2}}$ and $\overset{2}{\sim}\overline{\varrho_{NO_2}}$, but here the peak of the origin, $\overset{2}{\sim}\overline{\varrho_{NO_2}}$, is repeated along the polar axis, since correlations have been introduced. The

* Details of calculations are given in § 4.

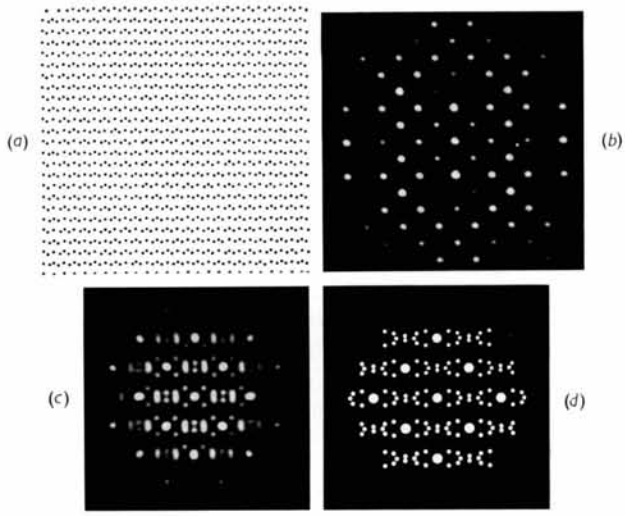

Fig. 5. Ferroelectric phase of $NaNO_2$, (100) projection. (*a*) Model of the ideal crystal lattice. (*b*) Optical reciprocal lattice. (*c*) Optical Patterson function. (*d*) Calculated Patterson function.

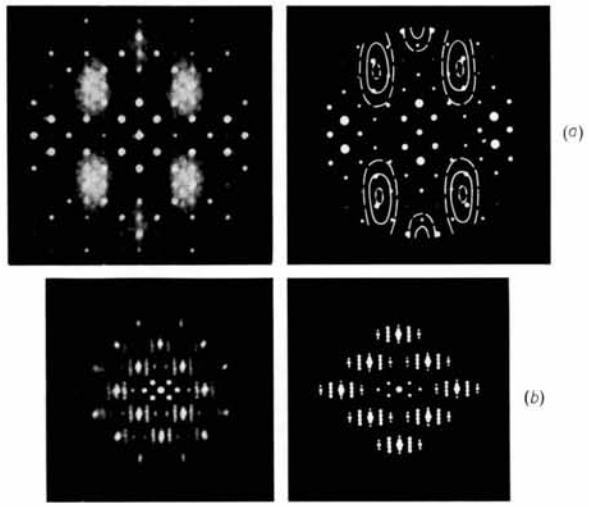

Fig. 6. (*a*) The diffraction patterns and (*b*) the *Q* function of the NO_2 groups in random distribution along the polar axis. Left: optical. Right: calculated.

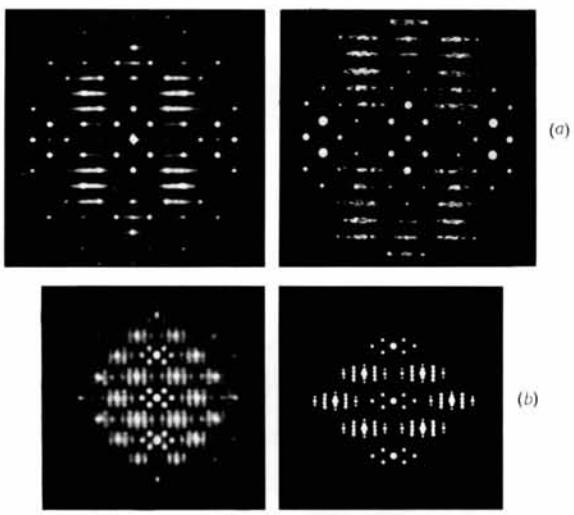

Fig. 7. (*a*) The diffraction patterns and (*b*) the *Q* function of the NO_2 groups. Correlations along the polar axis have been introduced. Left: optical. Right: calculated.

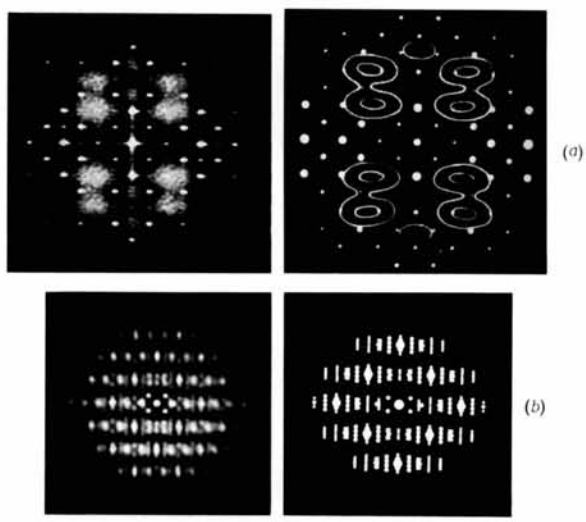

Fig. 8. (*a*) The diffraction patterns and (*b*) the *Q* function of the (100) projection of $NaNO_2$. Random distribution of NO_2 groups, but a statistical positional correlation to the Na ions along the polar axis. Left: optical. Right: calculated.

[*To face p.* 976]

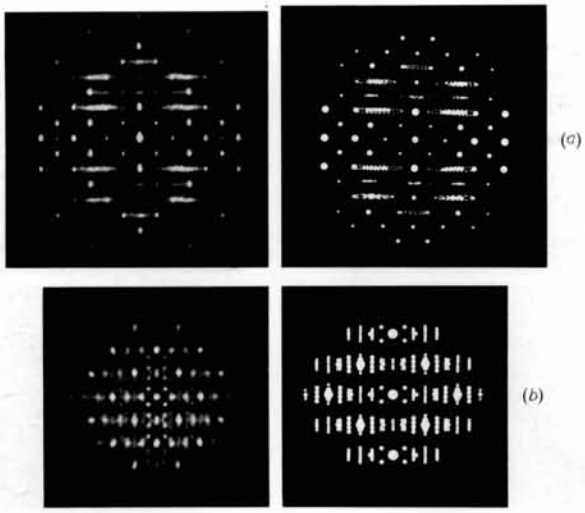

Fig. 9. (*a*) The diffraction patterns and (*b*) the *Q* function of the (100) projection of $NaNO_2$. Correlations along the polar axis have been introduced. Left: optical. Right: calculated.

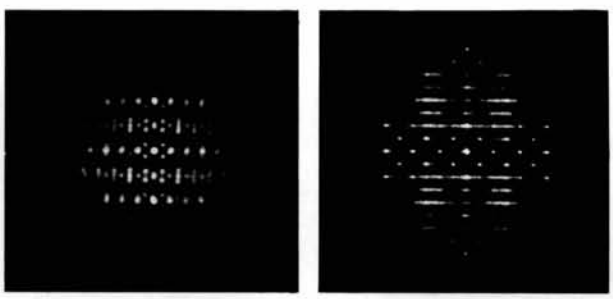

Fig. 11. (*a*) The *Q*-function and (*b*) Fraunhofer pattern of the paraelectric phase of $NaNO_2$, (100) projection. Rigid body motion of the 'cigarrillos' along the polar axis (with $\tilde{u}_{[001]} \sim 0{\cdot}2$ Å).

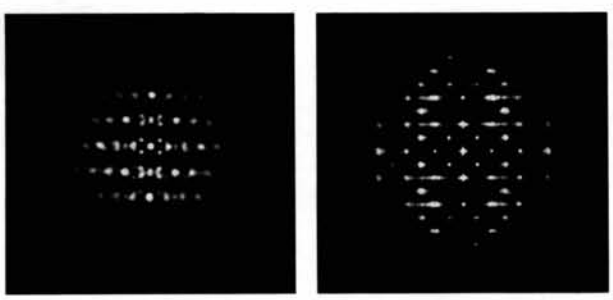

Fig. 12. (*a*) The *Q*-function and (*b*) Fraunhofer pattern of the paraelectric phase of $NaNO_2$, (100) projection. Rigid body motion of the positive and negative statistical domains along the polar axis ($\tilde{u}_{[001]} \sim 0{\cdot}20$ Å) plus transverse motion ($\tilde{u}_{[010]} \sim 0{\cdot}20$ Å) of quadratical segments.

remaining peaks correspond to $\overset{2}{\varrho}_{NO_2}$. Instead of (1) now the remaining difference term is given by

$$[\Delta\overset{2}{\varrho}_{NO_2}]\,\widehat{.}\,\overset{2}{z}s_{cig}\,. \tag{4}$$

The convolution product (symbol $\widehat{\ }$) is defined both in Fourier and in physical space and given by

$$\widehat{G_1(\mathbf{b})G_2(\mathbf{b})} = \int G_1(\mathbf{c})\,G_2(\mathbf{b}-\mathbf{c})\,d\mathbf{c};\quad \widehat{g_1(\mathbf{x})g_2(\mathbf{x})} = \int g_1(\mathbf{y})\,g_2(\mathbf{x}-\mathbf{y})\,d\mathbf{y}\,.$$

$s_{cig}(\mathbf{x})$ is the shape function of the 'cigarrillo' and

$$z(\mathbf{x}) = \sum_{n=-\infty}^{\infty} P(x_3-nc) \tag{5}$$

a one-dimensional lattice peak function along the polar c axis. The vector $\mathbf{x}$ expands the physical space and has the orthogonal components $x_1\,x_2\,x_3$, respectively along x, y, z.

The diffuse intensity will be given by the Fourier transform of this difference term

$$I_{dif} = (1/c)\,[\Delta|F_{NO_2}|^2].\widehat{(Z.|S_{cig}|^2)} \tag{6}$$

where $Z(\mathbf{b})$ is the Fourier transform of $z(\mathbf{x})$ and $S_{cig}(\mathbf{b})$ the Fourier transform of $s_{cig}(\mathbf{x})$. If all cigarrillos have the same length L_{cig}, each consisting of N_{cig} NO_2 groups, the shape factor $|S_{cig}|^2$ of the cigarrillo is given by

$$|S_{cig}|^2 = \left(\frac{\sin\pi b_3 L_{cig}}{\pi b_3}\right)^2 \simeq L_{cig}^2\exp\left[-\frac{\pi^2 b_3^2 L_{cig}^2}{3}\right] \tag{7}$$

and hence

$$\frac{1}{c}\widehat{(Z|S_{cig}|^2)} = N_{cig}^2\sum_m \exp\left[-\frac{\pi^2 L_{cig}^2}{3}\left(b_3-\frac{m}{c}\right)^2\right]. \tag{8}$$

The reciprocal vector $\mathbf{b}$ is defined by Ewald's construction

$$\mathbf{b} = \frac{\mathbf{s}-\mathbf{s}_0}{\lambda}\,, \tag{9}$$

$\mathbf{s}$, $\mathbf{s}_0$ being unit vectors of the direction of the diffracted and primary X-ray beam, λ wavelength and b_1, b_2, b_3 the orthogonal components of $\mathbf{b}$.

From the width of the diffuse lines in direction b_3 one can easily calculate by equations (6)–(8) the average length L_{cig} of the cigarrillo-like domains.

Fig. 7(*a*) (right) shows the calculated isodiffusion lines in terms of equation (6). Fig. 7(*b*) (right) reproduces the central region of the calculated Q function.

The next step was to make the models of the real structure, *i.e.* by introducing the Na atoms. Two models, analogous to the ones with only NO_2 groups, were drawn in terms of the atomic coordinates given by Kay, Frazer & Ueda (1962), one with statistical random distribution of positive and negative groups along the polar axis, and the other with correlations along the polar axis. However, to some extent correlations in both models for the Na atoms were introduced. This was because, even in the model with random distribution of the NO_2 groups, statistical positive and negative domains appeared, since inside a statistical domain of positive NO_2 groups the Na atoms were all drawn as positive. The same criterion was taken for the negative domains. Finally, within the boundaries of the statistical domains, the Na atoms were located at half the distance of the two NO_2 groups, *i.e.* at $0\frac{1}{2}0$ and $\frac{1}{2}00$. Thus we have the following four constellations of our statistical model, each with the probability $\frac{1}{4}$:

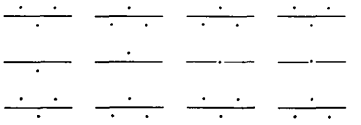

Fig. 8 shows the Fraunhofer patterns and Q functions of the paraelectric phase of $NaNO_2$, when such random distribution is assumed. The peak at the center of the Q function corresponds to $\overline{\overset{2}{\varrho}_{NO_2}+\overset{2}{\varrho}_{Na}}$ and again is different from the other peaks. Repeated by lattice translations 010, $0\frac{1}{2}\frac{1}{2}$, 001, 020, $0\frac{3}{2}\frac{1}{2}$, $\cdots$ there appear the motifs $\overset{2}{\varrho}_{NO_2}+\overset{2}{\varrho}_{Na}$. At half translations $0\frac{1}{2}0$, $01\frac{1}{2}$, $0\frac{1}{2}1$, $\cdots$ there appear the motifs $2[\widehat{\varrho_{NO_2}\varrho_{Na}}]$, except in the direction of the polar axis where at $00\frac{1}{2}$ and $00\bar{\frac{1}{2}}$ we have $2(\widehat{\varrho_{NO_2}\varrho_{Na}})$, which is not equal to $2(\widehat{\varrho_{NO_2}\varrho_{Na}})$.

Now instead of (1) the difference term of the Q function shows a hump at (000), given by

$$\Delta_1\overset{2}{\varrho} = \Delta\overset{2}{\varrho}_{NO_2}+\Delta\overset{2}{\varrho}_{Na}$$

and two other humps at $(00\frac{1}{2})$ and $(00\bar{\frac{1}{2}})$ given by

$$\Delta_2\overset{2}{\varrho} = 2[\overline{\widehat{\varrho_{NO_2}\varrho_{Na}}} - \widehat{\overline{\varrho_{NO_2}\varrho_{Na}}}]\,.$$

Figure 8(*b*) (left) clearly demonstrates the difference of the structure of the two humps at $(00\frac{1}{2})$ and $(00\bar{\frac{1}{2}})$ from that of the other mixed humps $2[\widehat{\varrho_{NO_2}\varrho_{Na}}]$ at $01\frac{1}{2}$ $0\frac{1}{2}1$ $0\frac{3}{2}0$ *etc.*

We now have four different motifs, two with correlations, two without correlations

at 000			at $00\pm\frac{1}{2}$		
1	1		$\frac{1}{2}$	$\frac{1}{2}$	$\frac{1}{2}$
1	4	1	$\frac{1}{2}$	$\frac{1}{2}$	$\frac{1}{2}$
1	1		$\frac{1}{2}$	$\frac{1}{2}$	$\frac{1}{2}$
			$\frac{1}{2}$	$\frac{1}{2}$	$\frac{1}{2}$

at $01\frac{1}{2}, 0\frac{1}{2}0, \cdots$

	$\frac{1}{4}$	
$\frac{1}{4}$	$\frac{1}{2}$	$\frac{1}{4}$
$\frac{1}{2}$	$\frac{1}{4}$	$\frac{1}{2}$
$\frac{1}{2}$	–	$\frac{1}{2}$
$\frac{1}{2}$	$\frac{1}{4}$	$\frac{1}{2}$
$\frac{1}{4}$	$\frac{1}{2}$	$\frac{1}{4}$
	$\frac{1}{4}$	

at $001, 0\frac{1}{2}\frac{1}{2}, \cdots$

		$\frac{1}{4}$		
	$\frac{1}{2}$	–	$\frac{1}{2}$	
$\frac{1}{4}$	$\frac{1}{2}$	$\frac{1}{2}$	$\frac{1}{2}$	$\frac{1}{4}$
$\frac{1}{2}$	–	$\frac{5}{2}$	–	$\frac{1}{2}$
$\frac{1}{4}$	$\frac{1}{2}$	$\frac{1}{2}$	$\frac{1}{2}$	$\frac{1}{4}$
	$\frac{1}{2}$	–	$\frac{1}{2}$	
		$\frac{1}{4}$		

The diffuse scattering will be given by Fourier transformation of these two difference terms. Taking into account that the $\Delta_2\underset{\sim}{\overset{2}{\varrho}}$ humps lie at $00\frac{1}{2}$ and $00\bar{\frac{1}{2}}$, we get

$$I_{\text{dif}} = \Delta|F^2_{NO_2}| + \Delta|F^2_{Na}| + 2\Delta|F_{NO_2}.F_{Na}|\cos\pi b_3 c\,. \quad (10)$$

The calculated isodiffusion lines in terms of the above equation are shown in Fig. 8(*a*) (right). As shown in § 4, the first two terms of equation (10) give rise to diffuse background as in Fig. 6, where a broad diffuse hump lies in the area of (034). The last term of equation (10) has negative values for the layers $l=1, 3$ in the domains of this hump. So this hump in Fig. 8(*a*) is split into two peaks. The correlation between adjacent Na and NO_2 groups, introduced into the model of Fig. 7, though relatively weak, produces a large effect on the background scattering, which can easily be analysed.

A striking resemblance can easily be seen between the continuous diffuse regions appearing in the Fraunhofer pattern and the X-ray diffuse scattering of molecular crystals, which also can be computed in terms of a difference Fourier transform approach (Amorós, Canut & de Acha, 1960). The fact that the X-ray scattering of the paraelectric phase of $NaNO_2$ shows diffuse sheets distributed normal to the polar axis proves that a random distribution of the NO_2 and the above mentioned small correlation of the Na groups cannot account for the observed X-ray diffuse scattering. Some kind of correlation must be considered along the polar axis, which acts over larger distances than the correlation introduced in Fig. 8. From the widths of the X-ray diffuse sheets, it is easily seen that a statistical unit consisting of about five NO_2 and Na groups along the polar axis must exist. Such long rod-like domains with inner correlation (cigarrillos) were taken for the next model. Its Fraunhofer pattern and corresponding Q function are represented in Fig. 9. The Q function only differs from the Q function of the last model in the fact that the peaks at the origin and at $00\frac{1}{2}$ and $00\bar{\frac{1}{2}}$ are repeated about five times by lattice translation along the polar axis, owing to the introduction of correlations. Since within each cigarrillo the positions $00\frac{1}{2}$, $00\bar{\frac{1}{2}}$ of Na atoms of model Fig. 8 do not occur, the last term of equation (10) must be multipled by 2*.

* See § 4 for further details.

The Fraunhofer pattern of Fig. 9(*a*) clearly shows the desired thin sheets, lying along rows of l=integer in the areas where the continuous diffuse sheets of the random model appeared. The diffuse intensity can be expressed in terms of the following equation:

$$I_{\text{I}} = (1/c)[\Delta|F_{NO_2}|^2 + \Delta|F_{Na}|^2 + 4\Delta|F_{NO_2}.F_{Na}|\cos\pi b_3 c].Z|\widehat{S_{\text{cig}}}|^2\,. \quad (11)$$

The isodiffusion lines calculated by the above formula are shown in Fig. 9(*a*) (right).

As shown in § 4, for $l=2, 4, 5, \Delta(F_{NO_2}F_{Na})$ has positive values for $k\sim 3$ and negative values for $k=0$. Hence equation (8) gives rise to strong diffuse lines at $l=2, 4$ in agreement with the observed X-ray diffuse scattering (Fig. 4*b*). However, the main difference is seen around the reciprocal lattice point 002, 004, where in the Fraunhofer pattern I_{I} according to (11) is zero and the Laue photographs show diffuse scattering. In order to check this point, X-ray diffractometric measurements were made along $l=2$, both at room temperature and at 185 °C (Fig. 10). The experimental fact can easily be seen that at 185 °C the diffuse scattering for $l=2$ is continuous from 002 up to at least 032 and is not zero at the forbidden reciprocal lattice points 012 and 032. Near to the Bragg reflexions 002 and 022 we observe the overlap of typical thermal diffuse scattering and disorder scattering.

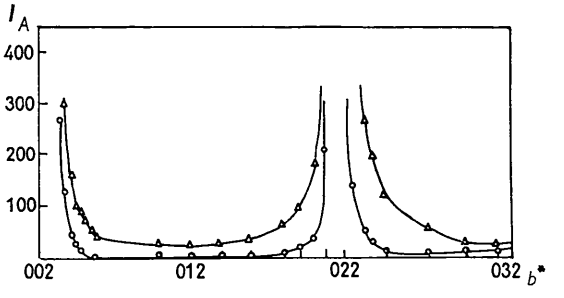

Fig. 10. Diffractometric measurements of the diffuse scattering from 002 to 032 at 20 °C and 185 °C. The experimental points measured are plotted as ○ and △ at room and high temperature, respectively (after Mendiola, 1964).

As shown in § 4, positional disorder never gives rise to diffuse layers at 002, 004. Uncorrelated thermal vibrations and librations of the single Na and NO_2 groups never produce diffuse layers. Correlated librations of the groups within a cigarrillo domain never produce a strong enough diffuse layer line near 002. Transforming the observed I_{dif} into the difference term hump of the unknown Q function, one finds out directly that the whole cigarrillos must oscillate as more or less rigid entities. Such motion moreover does not contradict the structural data of Kay & Frazer, since they found, from intensity data of reflexions at 185 °C, oscillation amplitudes for Na, N and O of about 0·2 Å.

A model was made with correlations along the polar axis, with the statistical unit cigarrillos as in the model of Fig. 9, but in this case subject to rigid body motions along the polar axis, with a mean vibrational amplitude of $\bar{u}_3=0{\cdot}20$ Å, as detected from neutron structural data. The Q function of this model is shown in Fig. 11(*a*), and the Fraunhofer pattern in Fig. 11(*b*). We can see in (*b*) that by means of this motion diffuse scattering through 002 appears. This new component of the diffuse intensity function is given by the following expression:

$$I_{II} = (1/c)[|\overline{F}_{NO_2}|^2+|\overline{F}_{Na}|^2 + 2|\overline{F_{NO_2}}|\,.\,|\overline{F_{Na}}|\cos\pi b_3 c].\widehat{Z|S_{cig}|^2}(1-D_3^2)\,. \quad (12)$$

$D_3^2=\exp[-4\pi^2 b_3^2\bar{u}_3^2]$ is the Debye factor of this anisotropic thermal motion of the whole cigarrillo; the bracket gives the average structure factor of a cigarrillo. Since this one-dimensional structure has not the extinction rules of the three-dimensional structure of Fig. 1, (12) gives rise to intensities at 'forbidden' reflexions. If bundles of cigarrillos would oscillate as rigid entities, we should have to replace the bracket of (12) by the ordinary structure factor of ferroelectric $NaNO_2$ and the one-dimensional lattice factor Z by a two- or three-dimensional one. Then at 012, contrary to Fig. 10, no diffuse layer scattering could occur. Hence the existence of linear entities oscillating as units is proved.

From the X-ray disorder diffuse scattering plotted in Fig. 4(*b*) it can be seen that, apart from the continuous diffuse lines of $l=$ const., there also appears some disorder diffuse scattering in the b^* axis, surrounding the reciprocal lattice points 030 and 040.

An attempt was next made to obtain weak diffuse scattering located at $0k0$, as given by the X-ray experiments. A model was made where vibrations normal to the polar axis were also introduced. The whole statistical positive and negative domains were again subjected to a rigid body motion up or down (again $\bar{u}_3=0{\cdot}2$ Å). In addition, each domain was divided into statistical (100) layers (so called 'segments'). These segments were chosen so that they all had a rectangular shape (Fig. 13*b*). Then they were subjected to a transverse rigid motion with $\bar{u}_2=0{\cdot}2$ Å. The Q function and the Fraunhofer pattern of such a model are shown in Fig. 12. These twist-like vibrations of the elongated statistical domains have given rise for the first time to diffuse scattering in the b^* axis, around 050 and 060.

The following equation can be used to compute the corresponding Fraunhofer pattern:

$$I_{III} = (1/bc)[\overline{F}_{NO_2}(1+\exp[\pi i(k+l)])+\overline{F}_{Na}(\exp[\pi ik] + \exp[\pi il])]^2.\widehat{Z_2|S_{seg}|^2}.(1-D_2^2)\,. \quad (13)$$

The bracket includes the ordinary structure factor and produces intensities only at $k+l=$ odd. Z_2 is the

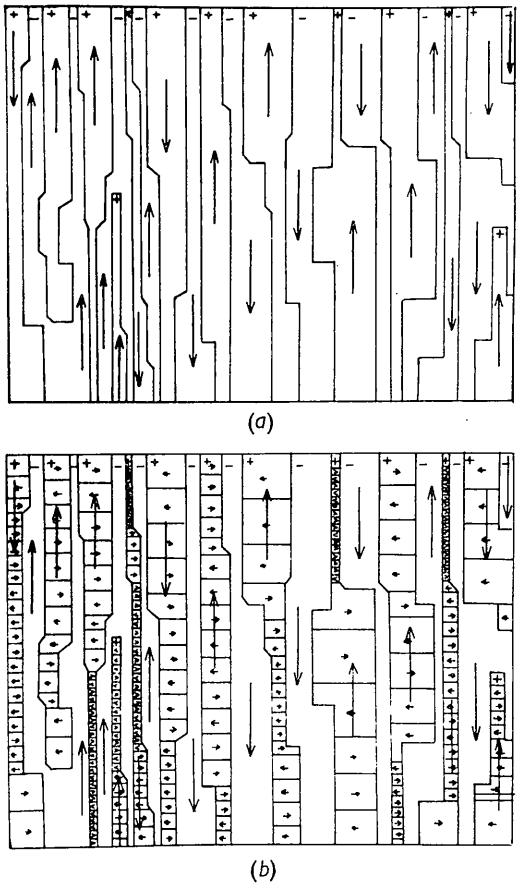

Fig. 13. A model with statistically distributed 25 Å long positive and negative cigarrillos. Domains of cigarrillos with the same sign occur statistically, which in the average consist of 5–10 cigarrillos. These domains as a whole are displaced statistically along the polar axis by $\pm 0{\cdot}02$ Å (*a*). Quadratical segments of the domains moreover are statistically displaced along the b axis by $\pm 0{\cdot}02$ Å (*b*).

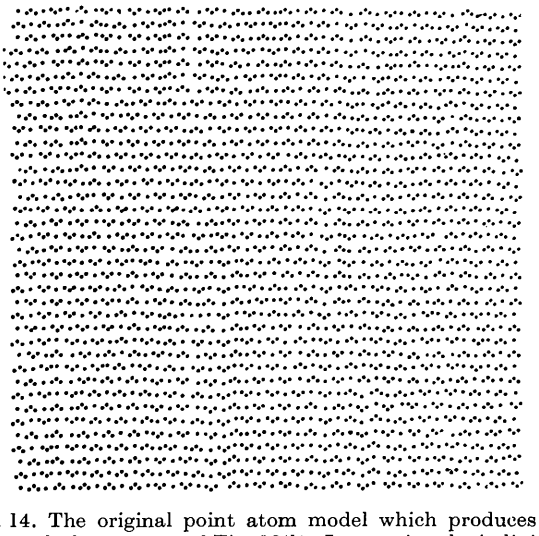

Fig. 14. The original point atom model which produces the Fraunhofer pattern of Fig. 12(*b*). It contains the individual ferroelectric 'oscillating' domains with 'twisting' segments of Fig. 13, frozen in their instantaneous positions.

two-dimensional lattice factor of all reflexions kl. $|S_{seg}|^2$ is the shape factor average of the segments. In Fig. 12(b) it has a globular shape, since the segments were globular too. Its width corresponds to the mean diameter of a segment width and in our statistical model was ~12 Å. The Debye factor

$$D_2^2 = \exp\left[-4\pi^2 b_2^2 \bar{u}_2^2\right]$$

of the horizontal segment oscillation depends only on b_2. The factor $1-D_2^2$ is zero near the 001 reflexions, which are all sharp, depending on the size of the whole model (~200 Å). But all other reflexions in Fig. 12 are surrounded by the diffuse spots of equation (13). The crystalline reflexions themselves are proportional to D_2^2 and can be seen in Fig. 12(b) only for all weak reflexions and the reflexions ($0l$) and (11) (20).

The observed X-ray diffuse spots appear at 030 and 040 and have a shape elongated in the polar direction. From this one directly learns that the segments, contrary to the model of Fig. 12, consist of single horizontal rows of NO_2–Na groups. Hence the bracket of (13) must be replaced by

$$|\overline{F_{NO_2}} + \overline{F_{Na}} \exp[\pi i k]|^2 \qquad (13a)$$

and the two-dimensional lattice factor by an one-dimensional lattice factor of a horizontal linear lattice. Then automatically the diffuse spot at 030 with a layer-like shape will appear as in Fig. 4(b).

If the vibrating segments consist of several horizontal $NaNO_2$ rows, the structure factor of (13) destroys the diffuse hump at 030. Since 030 exists we know that the segments are single horizontal rows.

Tanisaki (1961) carried out X-ray experiments just above the Curie point. The hkl reflexions show satellites at about $(h \pm \frac{1}{8}, kl)$; this he explains by antiphases (up and down structures) in the direction of the a axis, where about four groups are positive, and four negative, alternately. Since in our X-ray photographs the satellites no longer exist, this indicates that the correlation along the a axis is totally destroyed. So the cigarrillos consist also in the direction of the a axis of single statistically distributed rows, as fully established by the three-dimensional diffuse sheets normal to the polar axis, discussed above.

It follows from these results that the analysis of the diffuse scattering in the paraelectric phase of $NaNO_2$ can be given by a relative simple formula with three terms:

$$I_{dif} = I_I + I_{II} + I_{III} \qquad (14)$$

The first term depends on positional disorder only, the next on thermal vibrations of rod-like domains parallel to the polar axis, and the third on transversal vibrations of layer-like segments of domains in the [010] direction. The three terms are given by equations (11), (12), and (13) respectively, when the bracket of (13) must be replaced by (13a). In the following section they are calculated in detail, including correlated librations.

4. Calculation of correlated librations

The Q function of a single fixed NO_2 group consists of 7 discreet humps (see the central region of Fig. 6b). At (000) we have $\overset{2}{\sim}\varrho_N + 2\overset{2}{\sim}\varrho_O$, at the four positions $(\pm y_O, z_N - z_O)$ $(\pm y_O, z_O - z_N)$ we have $\widehat{\varrho_N \varrho_O}$ and at the two positions $\pm 2y_O$ we have $\overset{2}{\sim}\varrho_O$*. If the NO_2 group oscillates and librates, the outer six humps change their positions. If $H(y-\bar{y}, z-\bar{z})$ is the statistical distribution of the positional vector (y,z) around its average position $(\bar{y},\bar{z})$, H_{NO} the distribution function of the four humps, H_{OO} that of the two humps, and K_{OO} and K_{NO} the Fourier transforms of these functions, $K_{OO}(\mathbf{b}) = \mathfrak{F} H_{OO}(\mathbf{x})$, $K_{NO}(\mathbf{b}) = \mathfrak{F} H_{NO}(\mathbf{x})$, then the Fourier transform of the averaged Q function of the NO_2 group is given by

$$\begin{aligned}|\overline{F_{NO_2}}|^2 = {} & |F_N|^2 + 2|F_O|^2 + 4|F_N||F_O| K_{NO}(\mathbf{b}) \cos(s_2\bar{y}_O) \\ & \cos s_3(\bar{z}_O - \bar{z}_N) + 2|F_O|^2 K_{OO}(\mathbf{b}) \cos 2s_2\bar{y}_O \qquad (15)\end{aligned}$$

where $s_2 = 2\pi b_2$; $s_3 = 2\pi b_3$.

The averaged electron distribution of a 'positive' NO_2 group, on the other hand, is given by three humps, one with the ϱ_N density lying at $\bar{z}_N$, the two others with ϱ_O at $(\pm y_O, z_O)$. The humps of a 'negative' NO_2 group lie at $-\bar{z}_N$ and $(\pm y_O, -z_O)$. Introducing librations, the ϱ_O humps must be convoluted with H_O statistics, the ϱ_N hump with H_N statistics. If K_O, K_N are their Fourier transforms, we get

$$\begin{aligned}|\overline{F_{NO_2}}| = {} & |F_N| K_N(\mathbf{b}) \\ & \times \cos s_3\bar{z}_N + 2|F_O| K_O(\mathbf{b}) \cos s_2\bar{y}_O \cos s_3\bar{z}_O . \qquad (16)\end{aligned}$$

Hence the difference term, equation (3), is given by

$$\begin{aligned}\Delta F_{NO_2}^2 = {} & |F_N|^2 (1 - K_N^2(\mathbf{b}) \cos^2 s_3\bar{z}_N) + 2|F_O|^2 [1 + K_{OO}(\mathbf{b}) \\ & \times \cos 2s_2\bar{y}_O - 2K_O^2(\mathbf{b}) \cos^2 s_2\bar{y}_O \cos^2 s_3\bar{z}_O] \\ & + 4|F_N||F_O| [K_{NO}(\mathbf{b}) \cos s_2\bar{y}_O \cos s_3(\bar{z}_O - \bar{z}_N) \\ & - K_N(\mathbf{b}) K_O(\mathbf{b}) \cos s_2\bar{y}_O \cos s_3\bar{z}_O \cos s_3\bar{z}_N] . \qquad (17)\end{aligned}$$

If no librations occur, all factors $K(b) = 1$ and we obtain

$$\begin{aligned}\Delta F_{NO_2}^2 = {} & |F_N|^2 \sin^2 s_3\bar{z}_N + 4|F_O|^2 \cos^2 s_2\bar{y}_O \sin^2 s_3\bar{z}_O \\ & + 4|F_N||F_O| \cos s_2\bar{y}_O \sin s_3\bar{z}_O \sin s_3\bar{z}_N . \qquad (18)\end{aligned}$$

Equating the atomic scattering factors F_N^2, F_O^2 to unity, we obtain the formula which we have used to calculate the isodiffusion lines of Fig. 6(a) (right).

Introducing librations, the K factors of equation (17) with increasing $|\mathbf{b}|$ decrease from unity to zero. At large $|\mathbf{b}|$ values, one finds scattering like the gaseous type,

$$\Delta F_{NO_2}^2 = |F_N^2| + 2|F_O^2| . \qquad (19)$$

* $\varrho_O(\mathbf{x})$, $\varrho_N(\mathbf{x})$, $\varrho_{Na}(\mathbf{x})$ are the electron-density distributions of O, N and Na at zero point energy, if the centers of the atoms lie at $\mathbf{x}=0$, $\varrho^-(\mathbf{x}) = \varrho(-\mathbf{x})$.

According to the experimental results of Kay, Frazer & Ueda (1962) oscillation amplitudes not larger than $\bar{u}=0{\cdot}2$ Å are possible. Hence the K factors

$$K \simeq \exp[-2\pi^2\bar{u}^2b^2] \tag{20}$$

near the reflexion 002 have values so near to unity, that equation (18) holds as a good approximation and, hence, the isodiffusion lines of Fig. 6(a) (right) are correct for librating groups too, and can never explain the diffuse layer intensity near 002 (Fig. 10).

Things remain the same if we take into account librating Na ions. Then the second term of equation (11) is given by

$$\Delta F^2_{\mathrm{Na}} = |F^2_{\mathrm{Na}}|(1-K^2_a(\mathbf{b})\cos^2 s_2\bar{z}_a) \tag{21}$$

where $\pm\bar{z}_a=0{\cdot}04$ (Table 2) is the mean position of Na relative to the lattice point $(00\frac{1}{2})$ and $K_a(\mathbf{b})$ the Fourier transform of the libration statistics $H_a(\mathbf{x})$ around the positions $\bar{z}_a$.

Finally we calculate the last term of equation (11). Inside of a librating positive (negative) cigarrillo, $H_{\mathrm{AN}}, H_{\mathrm{AO}}$ may be the libration statistics of the distance vectors $\mathbf{x}_{\mathrm{Na}}-\mathbf{x}_{\mathrm{N}}, \mathbf{x}_{\mathrm{Na}}-\mathbf{x}_{\mathrm{O}}$ around their mean positions, and $K_{\mathrm{AN}}, K_{\mathrm{AO}}$ their Fourier transforms. Then the Q function has at $00\pm\frac{1}{2}$ two humps (see Fig. 8b) which consist of two density distributions $\widehat{\varrho_{\mathrm{Na}}\varrho_{\mathrm{N}}}\widehat{H}_{\mathrm{NA}}(z\pm(\bar{z}_{\mathrm{Na}}-\bar{z}_{\mathrm{O}}))$ at the positions $\pm(\bar{z}_{\mathrm{Na}}-\bar{z}_{\mathrm{N}})$ and four distributions $\widehat{\varrho_{\mathrm{Na}}\varrho}\widehat{H}_{\mathrm{AO}}(y\pm\bar{y}_{\mathrm{O}}, z\pm(\bar{z}_{\mathrm{Na}}-\bar{z}_{\mathrm{O}}))$ at the positions $\pm\bar{y}_{\mathrm{O}}, \pm(\bar{z}_{\mathrm{Na}}-\bar{z}_{\mathrm{O}})$.

The other corresponding humps of the Q function at $0, \pm\frac{1}{2}, 0$; $0, \pm1, \pm\frac{1}{2}$ have twelve humps, four at $\pm\bar{z}_{\mathrm{Na}}\pm z_{\mathrm{N}}$ with the density distribution $\frac{1}{2}\widehat{\varrho_{\mathrm{Na}}\varrho_{\mathrm{N}}}\widehat{H_{\mathrm{N}}H_{\mathrm{A}}}$, and eight at $\pm\bar{z}_{\mathrm{Na}}\pm\bar{z}_{\mathrm{O}}\pm\bar{y}_{\mathrm{O}}$ with the distribution $\frac{1}{2}\widehat{\varrho_{\mathrm{Na}}\varrho_{\mathrm{O}}}\widehat{H_{\mathrm{O}}H_{\mathrm{A}}}$. The difference of the Fourier transforms of the humps at $(00\frac{1}{2})$ and $(0\frac{1}{2}0)$ is therefore

$$\begin{aligned}2\Delta|F_{\mathrm{NO_2}}F_{\mathrm{Na}}| &= 2|F_{\mathrm{Na}}||F_{\mathrm{N}}|(K_{\mathrm{NA}}(\mathbf{b})\cos s_3(\bar{z}_{\mathrm{Na}}-\bar{z}_{\mathrm{N}})\\ &\quad - K_{\mathrm{N}}(\mathbf{b})K_{\mathrm{Na}}(\mathbf{b})\cos s_3\bar{z}_{\mathrm{Na}}\cos s_3\bar{z}_{\mathrm{N}})\\ &\quad + 4|F_{\mathrm{Na}}||F_{\mathrm{O}}|\cos s_2\bar{y}_{\mathrm{O}}[K_{\mathrm{AO}}(\mathbf{b})\cos s_3(\bar{z}_{\mathrm{Na}}-\bar{z}_{\mathrm{O}})\\ &\quad - K_{\mathrm{Na}}(\mathbf{b})K_{\mathrm{O}}(\mathbf{b})\cos s_3\bar{z}_{\mathrm{Na}}\cos s_3\bar{z}_{\mathrm{O}}]\end{aligned} \tag{22}$$

If no librations occur, all K factors are equal to unity and we obtain

$$\begin{aligned}2\Delta|F_{\mathrm{NO_2}}F_{\mathrm{Na}}| &= 2|F_{\mathrm{Na}}||F_{\mathrm{N}}|\sin s_3\bar{z}_{\mathrm{Na}}\sin s_3\bar{z}_{\mathrm{N}}\\ &\quad + 4|F_{\mathrm{Na}}||F_{\mathrm{O}}|\sin s_3\bar{z}_{\mathrm{Na}}\sin s_3\bar{z}_{\mathrm{O}}\cos s_2\bar{y}_{\mathrm{O}}.\end{aligned} \tag{23}$$

Since at $00\frac{1}{2}$ and $00\bar{\frac{1}{2}}$ of the Q function such a difference term exists, we have to multiply (23) by $2\cos\pi b_3c$. Introducing the lattice factor Z and shape factor S^2_{cig} of the cigarillos, we finally have equation (11) which was used to calculate the isodiffusion lines of Fig. 9(a). In the model of Fig. 8, half of the Na ions are at the position $z_{\mathrm{Na}}=0{\cdot}5$. Then equation (23) must be multiplied by $\cos\pi b_3c$ and we obtain equation (10), which was used to calculate Fig. 8(a) (right).

Since according to Table 2, in a positive domain $\bar{z}_{\mathrm{Na}}=+0{\cdot}04$, $\bar{z}_{\mathrm{N}}=+0{\cdot}07$, $\bar{z}_{\mathrm{O}}=-0{\cdot}04$, the first term of (23) is positive, the second negative. The same holds for negative domains. Hence the last term of equation (11) for $k\sim\pm3$ is positive for layer lines $l=2, 4, \cdots$ and negative for $l=3, 5$. In Fig. 9(a) (right), the layer lines $l=2, 4$ therefore, are strong near $k=\pm3$, while the layer line $l=\pm5$ is strong for $k=0$.

Introducing librations of any degree, one easily can see from equations (17), (21), (22), that no diffuse layer line can arise near 002. To obtain it, the whole cigarrillos must oscillate, as described in § 3.

The authors wish gratefully to acknowledge the valuable discussions and encouragement of Prof. J. L. Amorós and to express thanks to Fräulein Engel for assistance with the Fraunhofer patterns and optical Q functions.

References

Alonso, P., Canut, M. L. & Amorós, J. L. (1958). *Bol. R. Soc. Esp. Hist. Nat.* (G) **56**, 51.

Amorós, J. L. (1960). US Army Report. Contract DA-91-591-EUC-1084-01-1310-59.

Amorós, J. L., Alonso, P. & Canut, M. L. (1958). *Bol. R. Soc. Esp. Hist. Nat.* (G) **56**, 77.

Amorós, J. L., Canut, M. L. & de Acha, A. (1960). *Z. Kristallogr.* **114**, 39.

Carpenter, G. B. (1952). *Acta Cryst.* **5**, 132.

Carpenter, G. B. (1955). *Acta Cryst.* **8**, 852.

Hosemann, R. (1959). *Naturwissenschaften*, **46**,542.

Hosemann, R. & Bagchi, S. N. (1962). *Direct Analysis of Diffraction by Matter*. Amsterdam: North Holl. Publ. Co.

Kay, M. I. & Frazer, B. C. (1961). *Acta Cryst.* **14**, 56.

Kay, M. I., Frazer, B. C. & Ueda, R. (1962). *Acta Cryst.* **15**, 506.

Mendiola, J. (1964). Thesis, Madrid University. In preparation.

Mitsui, T. (1958). Seminar talk at the Massachusetts Institute of Technology, December.

Sawada, S., Nomura, S., Fujii, S. & Yoshida, I. (1958). *Phys. Rev. Letters*, **1**, 320.

Strijk, B. & MacGillavry, C. H. (1943). *Rec. trav. chim. Pays-Bas*, **62**, 705.

Strikj, B. & MacGillavry, C. H. (1946). *Rev. trav. chim. Pays-Bas*, **65**, 127.

Tanisaki, S. (1961). *J. Phys. Soc. Japan*, **16**, 579.

Truter, M. R. (1954). *Acta Cryst.* **7**, 73.

Ziegler, G. E. (1931). *Phys. Rev.* **38**, 1040.